Supporting Information for

# Nonadiabatic molecular dynamics simulations shed light on the timescale of furylfulgide photocyclisation

Michał Andrzej Kochman[†,‡]

[†] Institute of Physical Chemistry, Polish Academy of Sciences, Ul. Marcina Kasprzaka 44/52, 01-224 Warsaw, Poland
[‡] Theoretical Chemistry, Ruhr University Bochum, Universitätsstraße 150, 44801 Bochum, Germany
e-mail: mkochman@ichf.edu.pl

## Contents

## S1 $E_\alpha \rightleftharpoons E_\beta$ equilibrium of furylfulgide *t*Bu-1

As mentioned in the Background section in the main body of this paper, furylfulgides in the series **1** each possess two *E*-type isomers, conventionally termed the $E_\alpha$ and $E_\beta$ isomers, which differ in the orientation of the 2,5-dimethyl-3-furyl moiety. For reference, the geometries of the $E_\alpha$ and $E_\beta$ isomers of *t*Bu-**1** are compared in Figure S1. In the solution phase, the two isomers exist in thermodynamic equilibrium with one another. To the best of my knowledge, their relative abundances have not been determined experimentally. Accordingly, I undertook to estimate them on the basis of electronic structure calculations.

**Figure S1:** Visual comparison of the geometries of the $E_\alpha$ (drawn in blue) and $E_\beta$ (red) isomers of furylfulgide *t*Bu-**1**, as optimised at the B3LYP-D3(BJ)/def2-TZVP level of theory (see below for simulation parameters). The geometries were overlaid on one another in such a way as to minimise the root-mean-square distance between heavy atoms which do not belong to the 2,5-dimethyl-3-furyl moiety.

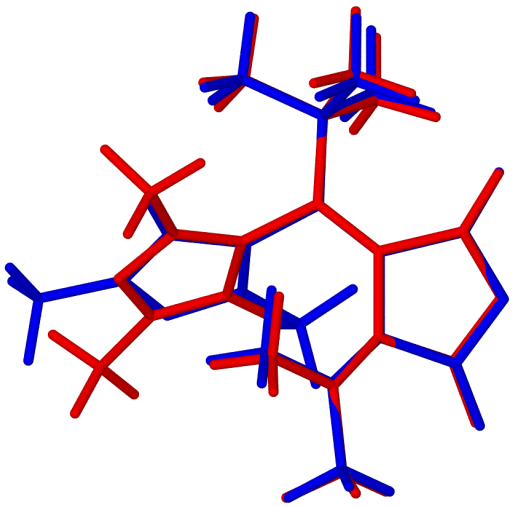

The computational methodology was analogous to that used in my and my coworkers' earlier study on the photorelaxation dynamics of Me-**1**.[1] Namely, the relative energies and free energies of the two isomers were calculated at the density functional theory (DFT) level. Because calculated thermochemical quantities depend on the choice of exchange-correlation functional, I performed the calculations with the use of several functionals: the pure generalised gradient approximation (GGA) functional B97-D3,[2] the global hybrid GGA functional B3LYP,[3,4] the meta-GGA functional TPSS[5] and the global hybrid meta-GGA functionals PW6B95[6] and M06-2X.[7]

The DFT calculations were performed in the computational chemistry software package Gaussian 16, Revision A.03.[8] At all times, I employed the def2-TZVP basis set[9] and the superfine integration grid implemented in Gaussian 16. In the case of the functionals B3LYP, B97-D3, TPSS, and PW6B95, the calculated energies and gradients were corrected for dispersion effects via the 'D3' semiempirical correction scheme of Grimme and coworkers with Becke-Johnson damping.[10] The inclusion of the dispersion corrections is noted by

adding the suffix -D3(BJ). When calculating the free energy difference between the two isomers, the temperature was set to 298 K. Solvent effects were not included in the calculations.

As a verification of the predictions of the DFT method, the single-point energies of the $E_\alpha$ and $E_\beta$ isomers of *t*Bu-**1** were re-calculated with the use of the domain-based local pair natural orbital (DLPNO) variant[11,12] of the coupled cluster with perturbative triples (CCSD(T)) method.[13] The DLPNO-CCSD(T) calculations were performed at equilibrium geometries optimised with the B3LYP-D3(BJ) functional. Afterwards, zero-point vibrational energy corrections and the thermal contributions to Gibbs free energy were taken from the B3LYP-D3(BJ) calculation. This composite level of theory is denoted DLPNO-CCSD(T)//B3LYP-D3(BJ).

The DLPNO-CCSD(T) calculations were carried out with the program Orca, version 4.2.1.[14,15] A restricted Hartree-Fock (RHF) reference determinant was used. The jun-cc-pVTZ basis set[16] was employed. I imposed the resolution-of-the-identity (RI) approximation for the calculation of both Coulomb integrals and exchange integrals, with the standard the standard aug-cc-pVTZ/C and aug-cc-pVTZ/JK auxiliary basis sets from the Orca basis set library.

The results of the calculations are summarised in Table S1. All five functionals with which the calculations were performed agree in predicting that the $E_\beta$ isomer lies higher in energy, and in Gibbs free energy, than the $E_\alpha$ isomer. The calculated Gibbs free energy differences fall in a narrow range from 6.1 kJ/mol (the value obtained in the composite DLPNO-CCSD(T)//B3LYP-D3(BJ) calculation) to 7.9 kJ/mol (the value from the B3LYP-D3(BJ) and the TPSS-D3(BJ) functionals).

The composite DLPNO-CCSD(T)//B3LYP-D3(BJ) level of theory predicts a smaller energy difference, and a smaller Gibbs free energy difference, than do the DFT calculations, but even with that method, the $E_\alpha \rightleftharpoons E_\beta$ equilibrium is predicted to be dominated by the $E_\alpha$ isomer. It follows that the population of the $E_\beta$ isomer is on the order of a few per cent.

**Table S1:** Values of energy difference ($\Delta E = E(E_\beta) - E(E_\alpha)$) and Gibbs free energy difference ($\Delta G = G(E_\beta) - G(E_\alpha)$) for the $E_\alpha \rightleftharpoons E_\beta$ isomerisation of furylfulguide *t*Bu-**1**. The energy difference includes zero-point vibrational energy corrections. $x(E_\alpha)$ is the estimated mole fraction of the $E_\alpha$ isomer at equilibrium.

| Level of theory | $\Delta E$, kJ/mol | $\Delta G$, kJ/mol | $x(E_\alpha)$ |
|---|---|---|---|
| B97-D3(BJ) | 6.7 | 7.4 | 0.95 |
| B3LYP-D3(BJ) | 6.0 | 7.9 | 0.96 |
| TPSS-D3(BJ) | 7.1 | 7.9 | 0.96 |
| PW6B95-D3(BJ) | 5.8 | 6.9 | 0.94 |
| M06-2X | 5.4 | 6.4 | 0.93 |
| DLPNO-CCSD(T)[a] | 4.2 | 6.1 | 0.92 |

[a] DLPNO-CCSD(T)//B3LYP-D3(BJ) composite calculation.

## S2 Setup of nonadiabatic molecular dynamics simulations

In this section, I provide a detailed discussion of the nonadiabatic molecular dynamics (NAMD) simulations with which I modelled the photocyclisation reaction of furylfulgide *t*Bu-**1**. The overall simulation methodology was identical to that used previously in Ref. 1 to study the photorelaxation process of another furylfulgide, Me-**1**. This was to enable a direct comparison of the simulation results for the two compounds.

For the sake of clarity, the discussion is divided into three parts. The first part focuses on the electronic structure calculations which were integrated into the NAMD simulations. The second describes how the initial conditions for the NAMD simulations were generated. Finally, the third covers the implementation of the NAMD method.

### S2.1 Electronic structure calculations

In the course of the NAMD simulations, the electronic structure of the *t*Bu-**1** molecule was treated with the use of the spin-flip variant[17,18] of time-dependent density functional theory (SF-TDDFT). The SF-TDDFT calculations were performed in the program Q-Chem, version 5.1.2.[19,20] The reference state was the unrestricted Kohn-Sham triplet state. I employed the 50–50 exchange-correlation functional,[17] whose makeup is 50% Hartree-Fock + 8% Slater + 42% Becke for exchange, and 19% VWN + 81% LYP for correlation. Moreover, I used the standard 6-31G(d) basis set in combination with the default integration grid SG-1.[21]

Electronic states obtained with the SF-TDDFT method suffer from varying degrees of spin contamination.[17,18,22] This problem is intrinsic to SF-TDDFT, and it is not restricted to any one type of system. In extreme cases, it becomes difficult, or impossible, to determine which states are singlets, and which are triplets (assuming a high-spin triplet reference state). Fortunately, in the case of furylfulgides, it has previously been shown that the spin contamination of the lowest few states ($S_0$, $S_1$, $S_2$, and $T_1$) is not too severe.[1]

During the NAMD simulations, I used the following automatic criterion to assign definite spin multiplicity (singlet or triplet character) to SF-TDDFT states. At each time step of each trajectory, I calculated the three lowest-energy SF-TDDFT states at the current nuclear geometry. The state with the highest expectation value of the total spin (i.e., highest $\langle S^2 \rangle$) was always identified as state $T_1$. The other two of the three states were identified as $S_0$ and $S_1$.

The NAMD simulation makes use of the nonadiabatic coupling vector (NACV) between states $S_0$ and $S_1$, which I calculated analytically, with the inclusion of electron translation factors, via the method of Zhang and Herbert.[23] As a measure to reduce the computational cost of the simulations, I started calculating the NACV only after the energy gap between states $S_0$ and $S_1$ in the given NAMD trajectory had decreased to below 0.5 eV. Once that had happened, I continued to calculate the NACV for the remainder of that trajectory (even after the energy gap increased to over 0.5 eV again). Neglecting the NACV during the initial part of the simulation, while the energy gap between states $S_0$ and $S_1$ is large, is justified by the fact that the magnitude of the NACV is inversely proportional to the energy gap between the two states.

## S2.2 Initial conditions

In order to generate the initial conditions for the NAMD simulations, I optimised the ground-state equilibrium geometry of the $E_\alpha$ isomer of furylfulgide *t*Bu-**1** at the DFT level of theory. In this calculation, the settings of the DFT method were the same as in the SF-TDDFT calculations (see Section S2.1 above), except that the restricted Kohn-Sham formalism was used. Afterwards, I calculated the vibrational modes of the molecule numerically.

Finally, I sampled $N_{\text{trajs}} = 50$ sets of nuclear positions and velocities from the harmonic oscillator Wigner distribution, and used them as the initial conditions for the NAMD dynamics. This approach is the de facto standard in NAMD simulations; its use is justified by the fact that the molecule is imparted with zero-point vibrational energy.[24,25] However, it also leads to a certain simulation artifact: the zero-point energy tends to "leak" from the high-frequency modes (especially hydrogen-heavy stretching modes) into low-frequency modes.[26–28] The problem can potentially become very severe for a hydrogen-rich molecule, such as *t*Bu-**1**. In order to mitigate the leakage of zero-point energy, I froze all of the C–H stretching modes when generating the Wigner distribution.

The initially occupied electronic state in each trajectory was $S_1$, and its population (in the context of the fewest switches surface hopping algorithm, see below) was set to unity.

## S2.3 NAMD simulations

This section covers the setup of the NAMD simulations. The time-evolution of the *t*Bu-**1** molecule was propagated with the fewest switches surface hopping[29,30] (FSSH) algorithm. In this method, the nuclear wavepacket of the system is represented by an ensemble of mutually independent semiclassical trajectories. In each trajectory, the nuclei are described by means of classical mechanics, while the electronic structure of the molecule is treated quantum mechanically.

In the FSSH algorithm, the wavefunction $\Psi(\mathbf{r}, t; \mathbf{R})$ of the electrons along a given nuclear trajectory $\mathbf{R} = \mathbf{R}(t)$ is expressed in terms of a linear combination of adiabatic states $\{\psi_j(\mathbf{r}; \mathbf{R})\}$ with time-dependent complex coefficients $\{a_j(t)\}$:

$$\Psi(\mathbf{r}, t; \mathbf{R}) = \sum_j a_j(t)\, \psi_j(\mathbf{r}; \mathbf{R}) \tag{1}$$

$|a_j(t)|^2$, the square modulus of the coefficient of the $j$-th state, is interpreted as the population of that state in the given trajectory.

The requirement that $\Psi(\mathbf{r}, t; \mathbf{R})$ satisfies the time-dependent electronic Schrödinger equation leads to a system of coupled differential equations for the time-evolution of the expansion coefficients:

$$\mathrm{i}\hbar\dot{a}_k = \sum_j a_j \left(\delta_{kj} E_k(\mathbf{R}) - \mathrm{i}\hbar\dot{\mathbf{R}} \cdot \mathbf{d}_{kj}\right) \tag{2}$$

where $\delta_{jk}$ denotes the Kronecker delta, $E_k(\mathbf{R})$ is the potential energy surface (PES) of the $k$-th adiabatic state, and $\mathbf{d}_{kj}$ is the NACV between states $k$ and $j$:

$$\mathbf{d}_{kj} = \langle \psi_k(\mathbf{r}; \mathbf{R}) \,|\, \nabla_{\mathbf{R}} \,|\, \psi_j(\mathbf{r}; \mathbf{R}) \rangle \tag{3}$$

In each simulated trajectory, at any given time, one adiabatic state $n$ from among those included in the linear expansion 1 is singled out as the occupied state (or, the current state). The nuclei move according to the classical equations of motion on the PES of that state:

$$\ddot{\mathbf{R}}_A = -\frac{1}{M_A} \nabla_A E_n(\mathbf{R}) \tag{4}$$

Note that, in the present case, the simulation does still include some nuclear quantum effects, albeit in an ad hoc fashion: the initial conditions for the dynamics include zero-point vibrational energy in most of the vibrational modes.

Nonadiabatic effects are accounted for by allowing a trajectory to undergo a switch (or "hop") between the current state and another adiabatic state, which then becomes the new current state for the given trajectory. The switches are imposed stochastically according to the criterion proposed by Tully.[29] This algorithm is designed in such a way as to ensure that the number of trajectories occupying each state is proportional to its population as defined by $|a_j(t)|^2$, and to achieve this goal with the lowest possible number of switches.

One also defines the classical populations of the adiabatic states included in the linear expansion 1. The classical population $P_j(t)$ of the $j$-th such state is defined as the fraction of trajectories that is currently evolving in that state:

$$P_j(t) = \frac{N_j(t)}{N_{\text{trajs}}} \tag{5}$$

As an illustration of the functioning of the FSSH algorithm, Figure S2 on the following page shows it being used to describe internal conversion in a two-state system. For the sake of simplicity, I am considering only a single simulated trajectory. The system starts out occupying the upper adiabatic state (state 2). Initially, the population of state 2 is set to unity, while the population of state 1 is set to zero. Internal conversion takes place while the system traverses an avoided crossing between states 1 and 2. In the vicinity of the avoided crossing, the two states exhibit strong nonadiabatic coupling, such that most of the population is transferred from state 2 to state 1. As a result, at one point, the system undergoes a hop from state 2 to state 1. Afterwards, it continues to evolve in state 1.

In the present case, the linear expansion 1 only included states $S_0$ and $S_1$. The system of equations 2 was integrated with the use of the fourth-order Runge-Kutta method with a time step of 0.001 fs, using quantities interpolated linearly between successive classical steps. Moreover, the time-evolution of the expansion coefficients was corrected for decoherence via the scheme proposed by Granucci and Persico.[31] The decoherence correction constant was set to $C = 0.1\ E_\text{h}$ (hartree). The dynamics of the nuclei (equation 4) was propagated with the use of the velocity Verlet integrator with a time step of 0.5 fs.

The calculation of the $S_1$–$S_0$ NACV gives rise to a technical complication. Because the phases of electronic wavefunctions calculated by a quantum chemistry program such as Q-Chem are set arbitrarily, the direction of the NACV can (and does) change arbitrarily from one classical time step to another. In order to correct for this effect, the wavefunction phases were monitored by calculating the normalised dot products between NACVs calculated in successive time steps. Whenever a phase change was detected, the NACV was multiplied by $-1$ from that point onward.

**Figure S2:** Schematic illustration of the functioning of the FSSH method on the example of a two-state system. See text for details.

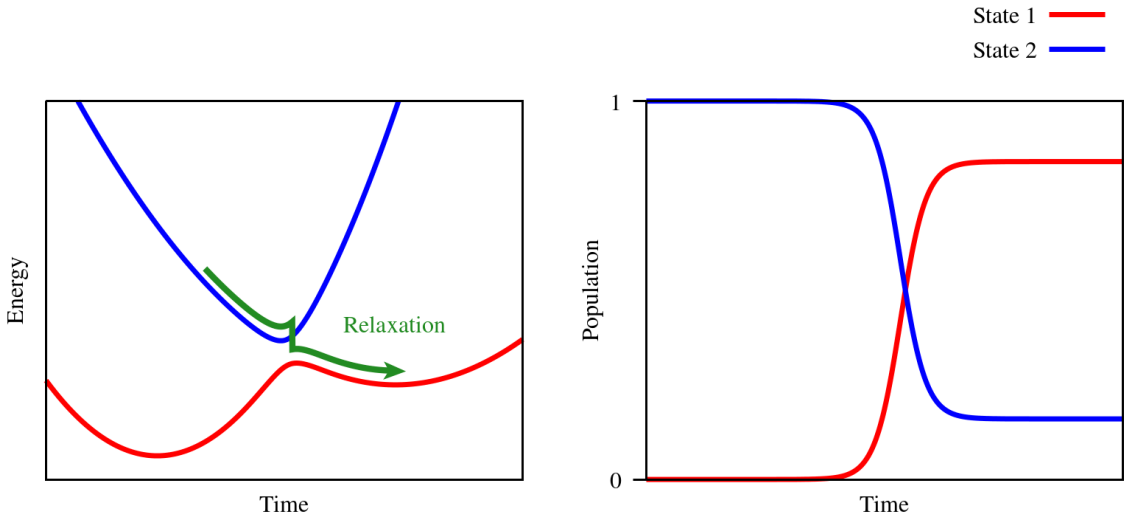


Whenever the molecule underwent a hop, the nuclear velocities were rescaled along the $S_1$–$S_0$ NACV if possible, and along the momentum vector otherwise.[32] In the event of a so-called "frustrated" hop – a situation where an upward hop cannot be imposed because it would be incompatible with energy conservation – the nuclear velocities were left unchanged.

## References


[1] M. A. Kochman, T. Gryber, B. Durbeej, A. Kubas, *Phys. Chem. Chem. Phys.*, 2022, **24**, 18103–18118.

[2] S. Grimme, *J. Comput. Chem.*, 2006, **27**, 1787–1799.

[3] A. D. Becke, *J. Chem. Phys.*, 1993, **98**, 5648–5652.

[4] P. J. Stephens, F. J. Devlin, C. F. Chabalowski and M. J. Frisch, *J. Phys. Chem.*, **1994**, **98**, 11623–11627.

[5] J. Tao, J. P. Perdew, V. N. Staroverov and G. E. Scuseria, *Phys. Rev. Lett.*, 2003, **91**, 146401.

[6] Y. Zhao and D. G. Truhlar, *J. Phys. Chem. A*, 2005, **109**, 5656–5667.

[7] Y. Zhao and D. G. Truhlar, *Theor. Chem. Acc.*, 2008, **120**, 215–241.

[8] Gaussian 16, Revision A.03, M. J. Frisch, G. W. Trucks, H. B. Schlegel, G. E. Scuseria, M. A. Robb, J. R. Cheeseman, G. Scalmani, V. Barone, G. A. Petersson, H. Nakatsuji, X. Li, M. Caricato, A. V. Marenich, J. Bloino, B. G. Janesko, R. Gomperts, B. Mennucci, H. P. Hratchian, J. V. Ortiz, A. F. Izmaylov, J. L. Sonnenberg, D. Williams-Young, F. Ding, F. Lipparini, F. Egidi, J. Goings, B. Peng, A. Petrone, T. Henderson, D. Ranasinghe, V. G. Zakrzewski, J. Gao, N. Rega, G. Zheng, W. Liang, M. Hada, M. Ehara, K. Toyota, R. Fukuda, J. Hasegawa, M. Ishida, T. Nakajima, Y. Honda, O. Kitao, H. Nakai, T. Vreven, K. Throssell, J. A. Montgomery, Jr., J. E. Peralta, F. Ogliaro, M. J. Bearpark, J. J. Heyd, E. N. Brothers, K. N. Kudin, V. N. Staroverov, T. A. Keith, R. Kobayashi, J. Normand, K. Raghavachari, A. P. Rendell, J. C. Burant, S. S. Iyengar, J. Tomasi, M. Cossi, J. M. Millam, M. Klene, C. Adamo, R. Cammi, J. W. Ochterski, R. L. Martin, K. Morokuma, O. Farkas, J. B. Foresman, and D. J. Fox, Gaussian, Inc., Wallingford CT, 2016.

[9] F. Weigend and R. Ahlrichs, *Phys. Chem. Chem. Phys.,* 2005, **7**, 3297–3305.

[10] S. Grimme, S. Ehrlich and L. Goerigk, *J. Comp. Chem.*, 2011, **32**, 1456–1465.

[11] Y. Guo, C. Riplinger, U. Becker, D. G. Liakos, Y. Minenkov, L. Cavallo and F. Neese, *J. Chem. Phys.*, 2018, **148**, 011101.

[12] D. G. Liakos, Y. Guo and F. Neese, *J. Phys. Chem. A* 2020, **124**, 90–100.

[13] K. Raghavachari, G. W. Trucks, J. A. Pople and M. Head-Gordon, *Chem. Phys. Lett.* 1989, **157**, 479–483.

[14] F. Neese, *Wiley Interdiscip. Rev. Comput. Mol. Sci.,* 2012, **2**, 73–78.

[15] F. Neese, F. Wennmohs, U. Becker and C. Riplinger, *J. Chem. Phys.*, 2020, **152**, 224108.

[16] E. Papajak, J. Zheng, X. Xu, H. R. Leverentz and D. G. Truhlar, *J. Chem. Theory Comput.,* 2011, **7**, 3027–3034.

[17] Y. Shao, M. Head-Gordon and A. Krylov, *J. Chem. Phys.*, 2003, **118**, 4807–4818.

[18] J. M. Herbert and A. Mandal, ChemRxiv, 2022.

[19] A. I. Krylov and P. M. W. Gill, *WIREs Comput. Mol. Sci.*, 2013, **3**, 317–326.

[20] Y. Shao, Z. Gan, E. Epifanovsky, A. T. B. Gilbert, M. Wormit, J. Kussmann, A. W. Lange, A. Behn, J. Deng, X. Feng, D. Ghosh, M. Goldey P. R. Horn, L. D. Jacobson, I. Kaliman, R. Z. Khaliullin, T. Kús, A. Landau, J. Liu, E. I. Proynov,

Y. M. Rhee, R. M. Richard, M. A. Rohrdanz, R. P. Steele, E. J. Sundstrom, H. L. Woodcock III, P. M. Zimmerman, D. Zuev, B. Albrecht, E. Alguire, B. Austin, G. J. O. Beran, Y. A. Bernard, E. Berquist, K. Brandhorst, K. B. Bravaya, S. T. Brown, D. Casanova, C.-M. Chang, Y. Chen, S. H. Chien, K. D. Closser, D. L. Crittenden, M. Diedenhofen, R. A. DiStasio Jr., H. Dop, A. D. Dutoi, R. G. Edgar, S. Fatehi, L. Fusti-Molnar, A. Ghysels, A. Golubeva-Zadorozhnaya, J. Gomes, M. W. D. Hanson-Heine, P. H. P. Harbach, A. W. Hauser, E. G. Hohenstein, Z. C. Holden, T.-C. Jagau, H. Ji, B. Kaduk, K. Khistyaev, J. Kim, J. Kim, R. A. King, P. Klunzinger, D. Kosenkov, T. Kowalczyk, C. M. Krauter, K. U. Lao, A. Laurent, K. V. Lawler, S. V. Levchenko, C. Y. Lin, F. Liu, E. Livshits, R. C. Lochan, A. Luenser, P. Manohar, S. F. Manzer, S.-P. Mao, N. Mardirossian, A. V. Marenich, S. A. Maurer, N. J. Mayhall, C. M. Oana, R. Olivares-Amaya, D. P. O'Neill, J. A. Parkhill, T. M. Perrine, R. Peverati, P. A. Pieniazek, A. Prociuk, D. R. Rehn, E. Rosta, N. J. Russ, N. Sergueev, S. M. Sharada, S. Sharmaa, D. W. Small, A. Sodt, T. Stein, D. Stück, Y.-C. Su, A. J. W. Thom, T. Tsuchimochi, L. Vogt, O. Vydrov, T. Wang, M. A. Watson, J. Wenzel, A. White, C. F. Williams, V. Vanovschi, S. Yeganeh, S. R. Yost, Z.-Q. You, I. Y. Zhang, X. Zhang, Y. Zhou, B. R. Brooks, G. K. L. Chan, D. M. Chipman, C. J. Cramer, W. A. Goddard III, M. S. Gordon, W. J. Hehre, A. Klamt, H. F. Schaefer III, M. W. Schmidt, C. D. Sherrill, D. G. Truhlar, A. Warshel, X. Xua, A. Aspuru-Guzik, R. Baer, A. T. Bell, N. A. Besley, J.-D. Chai, A. Dreuw, B. D. Dunietz, T. R. Furlani, S. R. Gwaltney, C.-P. Hsu, Y. Jung, J. Kong, D. S. Lambrecht, W. Liang, C. Ochsenfeld, V. A. Rassolov, L. V. Slipchenko, J. E. Subotnik, T. Van Voorhis, J. M. Herbert, A. I. Krylov, P. M. W. Gill and M. Head-Gordon, *Mol. Phys.*, 2015, **113**, 184–215.

[21] P. M. W. Gill, B. G. Johnson and J. A. Pople, *Chem. Phys. Lett.*, 1993, **209**, 506–512.

[22] Y. Horbatenko, S. Sadiq, S. Lee, M. Filatov and C. H. Choi, *Chem. Theory Comput.*, 2021, **17**, 848–859.

[23] X. Zhang and J. M. Herbert, *J. Chem. Phys.*, 2014, **141**, 064104.

[24] M. Barbatti and K. Sen, *Int. J. Quantum Chem.* 2016, **116**, 762–771.

[25] D. Avagliano, E. Lorini and L. González, *Phil. Trans. R. Soc. A*, 2021, **380**, 20200381.

[26] J. M. Bowman, B. Gazdy and Q. Sun, *J. Chem. Phys.*, 1989, **91**, 2859–2862.

[27] Y. Guo, D. L. Thompson and T. D. Sewell, *J. Chem. Phys.*, 1996, **104**, 576–582.

[28] S. Mukherjee and M. Barbatti, *J. Chem. Theory Comput.*, 2022, **18**, 4109–4116.

[29] J. C. Tully, *J. Chem. Phys.*, 1990, **93**, *1061–1071.*

[30] S. Hammes-Schiffer, J. C. Tully, *J. Phys. Chem.*, 1994, **101**, 4657–4667.

[31] G. Granucci, M. Persico, *J. Chem. Phys.*, 2007, **126**, 134114.

[32] A. Ferretti, G. Granucci, A. Lami, M. Persico and G. Villani, *J. Chem. Phys.*, 1996, **104**, 5517-5527.